Optimizing SERS From Gold Nanoparticle Clusters: Addressing The Near-field By An Embedded Chain Plasmon Model

Richard W. Taylor,[†] Rubén Esteban,[*,‡,¶] Sumeet Mahajan,[†] Javier Aizpurua,[‡] and Jeremy J. Baumberg[*,†]

NanoPhotonics Centre, Cavendish Laboratory, University of Cambridge, CB3 0HE, U.K., and Material Physics Center CSIC-UPV/EHU and Donostia International Physics Center DIPC, Paseo Manuel de Lardizabal 4 20018, Donostia-San Sebastián, Spain.

E-mail: ruben_esteban@ehu.eus; jjb12@cam.ac.uk

Abstract

We study experimentally and theoretically the optimization of surface enhanced Raman scattering (SERS) from nanoplasmonic clusters of gold nanoparticles separated by a fixed sub-nanometre gap. To maximize the enhancement we discuss how the optimal cluster size is influenced by the constituent nanoparticle size and illumination wavelength. We find good qualitative agreement between the experimental SERS from

[*]To whom correspondence should be addressed

[†]NanoPhotonics Centre, Cavendish Laboratory, University of Cambridge, CB3 0HE, U.K.

[‡]Material Physics Center CSIC-UPV/EHU and Donostia International Physics Center DIPC, Paseo Manuel de Lardizabal 4 20018, Donostia-San Sebastián, Spain.

[¶]Quantum Measurement Division and Joint Quantum Institute, National Institute of Standards & Technology and University of Maryland, Maryland 20899-8423, USA.

nanoparticle clusters and a simple composite model that describes the response of the full cluster as arising from a composition of linear nanochains. For fixed illumination wavelengths encountered experimentally, it is best to choose a cluster size that supports its lowest energy resonance near this wavelength. Our chain simulations indicate the existence of an optimal length also when the illumination laser is continuously tuned to the frequency that maximizes the signal. We explain the optimal length under these illumination conditions with a simple model that accounts explicitly for radiative losses.

Introduction

Self-assembling clusters of plasmonic nanoparticles are routinely harnessed for sensing applications when a localized and enhanced electric field is required at the nanoscale. Owing to the chemical inertness and biocompatibility of gold, as well as the large field enhancement which can be excited at optical wavelengths, gold nanoparticle clusters are widely used for a plethora of Surface Enhanced Raman Scattering (SERS)-based sensing strategies.

The resonant coupling of light to the free electrons within a gold nanoparticle (AuNP) leads to the localization and enhancement of the optical field in the form of a plasmon resonance. The coupling of such plasmons across a nano-junction gives rise to a strongly coupled resonance known as a *gap plasmon*.[1–3]

For SERS from nanoparticle clusters, large electromagnetic enhancements up to $\times 10^{10}$ are generated by gap plasmons within the nano-junctions.[4–6] The gap plasmon resonance and enhancement are exquisitely sensitive to the nanoparticle separation, with strongest enhancements for nano-scale gaps, and so efficient use for SERS benefits from control over the nano-junction gap width.[7] Moreover, the confinement of the fields to the small volume of the gap[3] can be exploited for highly localized sensing of a molecules at ultra-low concentration,[8–11]

and even single molecule detection.[12−18] Furthermore, more recent efforts have demonstrated the monitoring of chemical reactions localized *in situ* within the nano-gap via gap plasmon enhanced SERS,[19−20] and also mapping of individual molecules.[21]

In characterizing SERS from nanoparticle clusters, recent studies have examined individual aspects of the problem such as nanoparticle size, nano-junction width, cluster mass and peak optical extinction to identify the optimal features.[22−26] While SERS from plasmonic clusters is well established, a simple model to predict the nanocluster SERS is challenging, particularly for nanometric gaps much smaller than the particle diameter. A collective model that describes all factors is thus sought.[27] The inherent difficulty of interpreting SERS from the nanoparticle clusters lies primarily with the complicated quasi-fractal topology of the cluster itself. The measured SERS from the cluster arises in principle from the interactions between all aggregated particles within this random fractal arrangement. While full electromagnetic modeling is a possible route to a complete description of the plasmonics from the nanocluster,[28−32] such computations are challenging and the actual results pertinent to the precise nanocluster defined in the problem. In contrast, in experiments one often needs to account for a large ensemble average of nanoclusters whose morphology is only characterized via general descriptive parameters, and so an effective global description is desirable.[33]

In this work, we present systematic *in situ* Raman measurements of growing clusters of spherical particles illuminated at two different wavelengths and separated by narrow fixed gaps, to analyze the effect of both particle and aggregate-size upon the SERS signal. We interpret the experimental results using the embedded chain model (ECM), proposed in our previous work.[19,28] Further, we combine simulations with a simple semi-analytical model to analyse the influence of radiative losses on the SERS signal from chains illuminated at resonance.

An *embedded chain model* for nanocluster gap plasmons

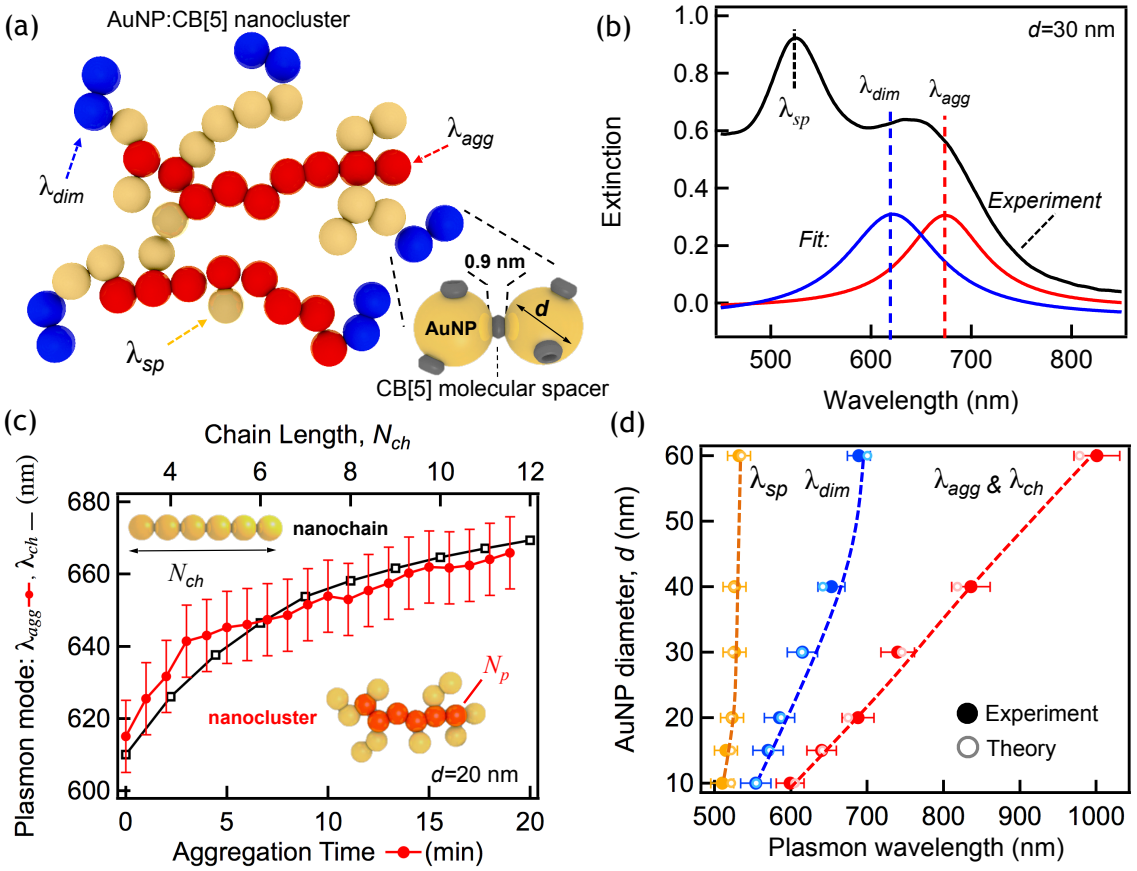

Figure 1: The embedded chain model interpretation for the plasmonics of a AuNP nanocluster cluster. (a) Illustration of the dendritic cluster topology with long chains (indicated by red color), peripheral dimers (blue) and single particle structures highlighted, with optical resonance λ_{agg}, λ_{dim} and λ_{sp} respectively. Inset: the CB[n] molecular linker fixes the separation between the particles to l_{gap}=0.9 nm throughout the cluster. (b) Measured extinction of an AuNP:CB[n] nanocluster solution (black), showing explicitly dimer (blue) and chain red modes depicted in (a) and resonant at λ_{dim} and λ_{agg}, respectively (obtained from fit). Particle diameter d=30 nm. An additional peak near the resonant wavelength λ_{sp} for the single spheres is also apparent. (c) The spectral evolution of the experimental long-wavelength resonance (λ_{agg}, solid circle) tracked during aggregation (bottom axis) for AuNP with d=30 nm. Also shown is the calculated plasmon resonance of a linear nanochain (λ_{ch}, open square) of the same diameter d and seperation l_{gap} as a function of particle length N_{ch} (top axis). (d) Resonant wavelength of the single particle (λ_{sp}), dimer (λ_{dim}) and chain (λ_{agg}) mode extracted from the experimental nanocluster for various diameter d, compared to the calculated values from linear chains of the same d and l_{gap} of length N_{ch}=1 (λ_{sp}), N_{ch}=2 (λ_{dim}) and N_{ch}=16 (λ_{ch}) respectively. Here, λ_{agg} corresponds to the observed lowest-energy plasmon following long aggregation times of the nanocluster. The error bars represent one standard deviation in the fitted peak position.

In this study, aggregation of AuNPs in water is induced by the addition of cucurbit[5]uril (CB[5]), where the CB[5] binds to the AuNP surface and acts as a rigid molecular spacer, defining the nano-junction separation to a rigid l_{gap} of around 0.9 nm throughout the cluster,[34–36] shown in the inset of Fig. 1(a). CB[5], and other members of the cucurbituril family, are hollow cages that are able to sequester analyte molecules within their interior.[37,38] This enables the analyte molecule to be localized to the very center of the gold nanoparticle gap, where the enhanced field is strongest. The topology of the nanoparticle cluster formed under diffusion-limited aggregation is depicted schematically in Figure 1(a) as a two-dimensional projection. Our previous measurements of these nanoclusters presented a motif of linear, branch-like extensions with sparse density that is characterized by a low fractal dimension.[34,39,40] We summarize here the *embedded chain model* (ECM) used to understand the numerous coupled gap plasmon resonances within these nanoclusters. This chain description is used in this paper to conceptualize and interpret the optimization of the SERS for various nanoparticle and cluster sizes and also Raman excitation wavelength.

Figure 1 presents a typical far-field extinction spectrum from a solution of AuNP:CB[5] nanoclusters (d=30 nm) produced using our previously reported methods.[34] Three distinct plasmonic features appear in the extinction at wavelengths labelled λ_{agg}, λ_{dim} and λ_{sp} in which $\lambda_{agg} > \lambda_{dim} > \lambda_{sp}$. Both λ_{agg} and λ_{dim} correspond to the central wavelength of two Lorenztians fitted to the extinction spectra following subtraction of the initial single particle resonance (pre-aggregation),[34] which shows a resonance at λ_{sp}=525 nm corresponding to the energy of the single-particle plasmon resonance. Further information on the preparation of the AuNP:CB[5] nano clusters can be found in the Supporting Information.

These three spectral features identified can be interpreted using the embedded chain model. In this framework, the cluster is described as a composite of non-interacting chains of different lengths, where these three different types of structures each contribute to the observed extinction [Figure 1(a)]. The longitudinal modes of the longer chains give rise to the longest

wavelength peak at λ_{agg}. Pairs of particles situated mostly at the exterior of the aggregate can act as optical dimers, giving a longitudinal plasmonic signature at λ_{dim}. Lastly, λ_{sp} is associated with single particles, either physically isolated or essentially uncoupled with the test of the cluster for a given polarization, or transverse modes of the chains.[34]

The long-wavelength mode of the nanocluster (which we refer to as the 'chain mode') is of particular interest for SERS as the resonance wavelength may be tuned across the visible range by controlling the extent of aggregation. The evolution of λ_{agg} during AuNP:CB[5] aggregation is presented in Figure 1(c, solid circle) for d=30 nm, in which a significant redshift in the plasmon mode is apparent, leading to an eventual saturation of the resonance wavelength. In the *ECM*, λ_{agg} is interpreted as arising from long-chain structures, where the redshift in wavelength corresponds to an increase in the length of the chains. Many disordered chains of different length should in principle contribute to the plasmonic response, but it is useful to interpret the features at λ_{agg} as the response of longitudinal modes of straight chains of a single effective length N_p and same gap separation distance l_{gap}=0.9 nm. Here, N_p is defined as the length of a straight chain with resonance λ_{ch} equal to λ_{agg}. It is thus particularly interesting to compare λ_{agg} with the resonant wavelength λ_{ch} of various particle lengths (N_{ch}).

The chain plasmon modes (λ_{ch}) calculated from a compositionally similar nanochain is presented in Figure 1(c, open square) for various chain lengths (N_{ch}). All the calculations in the paper are performed using the Boundary Element Method (BEM) assuming water as surrounding medium (permittivity ε_{wat}=1.77) and field polarization along the axis of the chains.[41,42] As desired, good correlation is found for the resonant wavelength of the long wavelength mode: λ_{agg} evolves with time in a similar manner as λ_{ch} evolves with the length of the chains, including the tendency for mode saturation towards a similar resonant wavelength (saturating for chains at N_{ch}=10-16).[43,44] Figure 1(d) illustrates the use of the *ECM* for different monomer diameters composing large AuNP:CB[5] clusters for which the nan-

ocluster growth is sufficient for λ_{agg} to be close to saturation. The cluster modes λ_{sp}, λ_{dim} and λ_{agg} obtained from the measurements agree well with the calculated values for a single sphere, a dimer and long chain (N_{ch}=16) respectively.[19]

Notably, to reach this agreement it was not necessary to consider in the calculations the significant disorder characterising self-assembled aggregates, because the optical response of chains appear to be rather insensitive to the presence of disorder in the form of moderate bends and kinks.[28] The coupled chain resonances do depend strongly on the widths of the gap and diameter of the particles, but the size distribution of these parameters is narrow and well controlled in the AuNP:CB[5] aggregates.

To summarize, while diffusion-limited clusters would contain chains of various lengths, we found it sufficient in the context of the *ECM* to consider just the longest grown chains associated with the measured long-wavelength plasmon mode (in addition to the contribution near λ_{sp} of the monomers and transverse modes and, most significantly, of the dimers resonant at $\approx\lambda_{dim}$ that are typically found at the periphery of the clusters).[28,45] We believe the *ECM* should be valid for different materials[32] and gap distances, at least as long as the structures are dendritic, the interaction sufficiently large and similar across all gaps, and the particles not too large ($d\lesssim$100 nm). The embedded chain model appears to be a useful framework to characterize the gap plasmons within dendritic nanoparticle clusters with well controlled gaps. In Figure 1, as in our previous work, the model was applied to far-field measurements. In the following we use the *ECM* to interpret the nanocluster SERS which originates from the near-field gap plasmon modes within the resonant nano-junctions.

Near-field response of nanochains

We first illustrate the behavior of the near field within the gaps by looking at simple linear nanochains of increasing length for d=30 nm [Fig. 2(a)].

The strong resonant fields are confined to the proximity of the chain with particularly strong local intensity at the gaps, as presented in Figure 2(b). We define the enhancement factor (EF) of a nano-junction gap plasmon at a particular gap as EF=($|E_{gap}|$ / $|E_0|$), where E_0 is the excitation field and E_{gap} the gap plasmon field in the center of the nano-junction. We obtain the *average* field enhancement ($\overline{EF}$) across all N_{ch}-1 nano-junctions of the nanochain at wavelength λ as:

$$\overline{EF}(\lambda) = \frac{1}{N_{ch}-1} \sum_{i=1}^{N_{ch}-1} \left| \frac{E_{gap,i}(\lambda)}{E_0(\lambda)} \right| \tag{1}$$

in which i denotes the *junction index*, the position of the gap along the chain.

The optimization can be divided into two schemes based on the choice for the excitation wavelength λ. In the first scenario we consider excitation at a *fixed* wavelength, a condition that is a common experimental constraint. Alternatively, we also consider the example where we excite each nanochain at its chain plasmon resonance, a condition we describe as being *perfectly tuned*. To quantify the match between excitation wavelength and plasmon mode we introduce the *detuning* parameter, Λ, defined as:

$$\Lambda = |\lambda - \lambda_{res}| \tag{2}$$

where λ_{res}=λ_{ch} for the nanochain, or λ_{res}=λ_{agg} for the experimental nanocluster. In principle, λ_{res} can be defined as the peak mode from either the far or the near field spectra; the choice should change the exact λ_{res} to only a small extent.[46–48] In this work, unless otherwise stated, we use the extinction peak, which can be easily obtained for both theory and experiment.

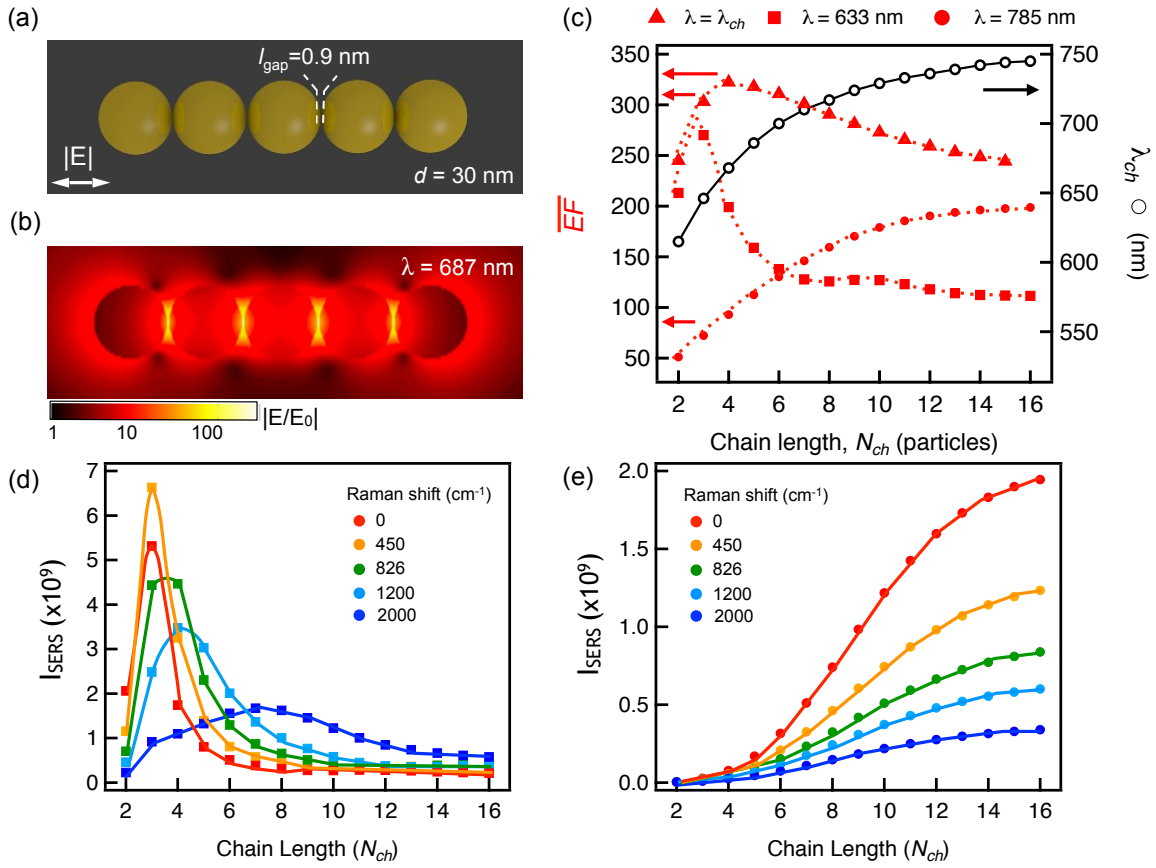

Figure 2: Near-field enhancement within a model nanochain. (a) Illustration of the nanochain geometry with incident electric field polarized parallel to the long chain axis. (b) Near-field map for a plane containing the axis of the chain, showing the electric near-field magnitude (normalized to the incident field and plotted in logarithmic color scale) for illumination at the longitudinal chain mode resonance (λ=687 nm). Strong enhancement is found at the interstitial gaps. (c) Average enhancement factor $\overline{EF}$ for the nanochain (solid markers, left axis) and corresponding mode wavelength (open marker, right axis) as a function of chain length N_{ch}. The enhancement presented is calculated for Raman illumination at λ=λ_{ch} (solid triangle), λ=633 nm (solid square) and λ=785 nm (solid circle). (d,e) SERS intensity as a function of chain length for various Stokes shifts with (d) λ=633 nm and (e) λ=785 nm. A particle diameter of d=30 nm is used throughout.

The mean field enhancement factor ($\overline{EF}$) as a function of N_{ch} for d=30 nm and the CB[5] particle spacing (l_{gap}=0.9 nm) is illustrated in Figure 2(c). We consider excitation at the longitudinal plasmon resonance of the chain (Λ=0 for all lengths, solid triangles), and at fixed wavelength of either λ=633 nm (solid squares) or 785 nm (solid circles). The resonant wavelengths for all lengths are also indicated (open circles), showing a monotonic increase that saturates for long chains.[43] In all cases, the $\overline{EF}$ remains relatively constant for $N_{ch} \gtrsim 10$, which can be linked to the saturation of the resonant wavelength λ_{ch} for these lengths.

For λ=633 nm, the optimization with N_{ch} is peaked around N_{ch}=3, the length for which the chain resonance is close to the illumination wavelength. For illumination in the near-infrared (NIR), λ=785 nm, the detuning diminishes with increasing N_{ch}, and the enhancement is optimized for the larger chains. Thus, for both fixed wavelengths it is convenient to tune the resonant frequency of the chain near the illumination wavelength to optimize $\overline{EF}$.

Perhaps more unexpectedly, the $\overline{EF}$, when under perfect tuning Λ=0 for all lengths, does not increase monotonically with a progressively longer chain, as might be expected. In the example of Figure 2(c), the optimal chain length is found to be a quadrameric chain ($N_{ch} = 4$). For the particular diameter d=30 nm considered here, the decrease for larger N_{ch} is small, with $\overline{EF}$ of the order $\approx$250 even for the sub-optimal long chains, which are still of practical use. We interpret below the presence of an optimal length as a consequence of non-radiative losses.

To conclude this example, we briefly exemplify the dependance of the SERS enhancement on the wavelength shift ν (in wavenumbers) induced by the Raman vibration. To a simple approximation, the Raman signal is proportional to the fourth power of the local electric field, but a better approximation considers the enhancement at both the illumination λ and the out-coupled λ'(here Stokes shifted) wavelength. We define the calculated SERS intensity

enhancement I_{SERS} as:

$$I_{sers} = \sum_{i=1}^{N_{ch}-1} \frac{1}{N_{ch}-1} \left| \frac{E_{gap,i}(\lambda)}{E_0(\lambda)} \right|^2 \left| \frac{E_{gap,i}(\lambda')}{E_0(\lambda')} \right|^2 \tag{3}$$

Here we again average over the contribution from each gap of the chain, where we have assumed that the photons from different junctions are emitted incoherently.[49,50]

For a large Stokes shift ν=2000 cm^{-1}, (encompassing the edge of the experimental Raman 'fingerprint' region), and with λ=600 nm-800 nm, the difference in energy of the incoming and scattered light would vary on the order of ≈15 %. This difference is comparable to the spectral width of the resonance from the nanochains, and thus we expect a moderate dependance of the SERS enhancement on the Stokes shift. To consider this dependance, the SERS calculated for several Stokes shifts from the model d=30 nm nanochains is presented in Figure 2(d,e).

In varying the Stokes shift ν the change in the SERS yield is indeed moderate for the two illumination frequencies considered, λ=633 nm [Figure 2(d)] and λ=785 nm [Figure 2(e)]. As a general feature, long chains are always favorable for λ=785 nm, i.e. for illumination to the red of the resonant peaks in Figure 2(c). For λ=633 nm the general qualitative behavior also remains similar for all Stokes shift, even when considering the largest shift ν=2000 cm^{-1}, but in this case the optimal length exhibits some dependance on ν. Larger ν require longer optimal chains so that the photons emitted at increasingly larger wavelengths are less strongly detuned with respect to the long chain resonances. The Stokes shift also modifies the strength of the emitted signal for both excitation wavelengths, but the change is generally smaller than one order of magnitude, which is relatively small in the context of SERS. In the following section we will consider a Stokes shift of ν=826 cm^{-1}, corresponding to a signature experimental CB[5] stretching mode.[51]

Optimizing SERS by minimizing detuning ($\Lambda \to 0$) for a fixed illumination wavelength

In this section, we examine optimization of SERS for a constraint of fixed illumination wavelength. We extend the example considered in Figure 2 to complex experimental AuNP:CB[5] nanoclusters of different sizes, applying the chain calculations and the *ECM* to interpret our measurements.

We measure the extinction from the AuNP:CB[5] nanocluster solution throughout aggregation and measure the integrated SERS signal of the aforementioned signature CB[5] Raman vibration mode to quantify the SERS enhancement (Supporting Information S2). The SERS signal is expected to be dominated by the CB[5] situated at the centre of the nano-junctions [Fig. 2(b)] where the enhanced field is strongest.

The long wavelength resonance of the nanocluster is related to the extent the nanoparticles are aggregated, which is itself related to the rate at which the particles coagulate. It should be noted that in Figure 3 the concentration of CB[5] used is lower than that used in Figure 1(d), to obtain a slower rate of aggregation (but still falling within the fast diffusion-limited regime), which facilitates possible the measurement of the SERS signal during the different stages of growth. Consequently, the chains within the growing aggregates do not necessarily reach the same lengths as before, which directly affects the maximum attained resonant wavelength as in Figure 1(d).

Following the *ECM*, we associate the long wavelength resonance of the nanocluster to a linear chain model. Thus, the experimental results for the growing clusters [Fig. 3(a,b)] are compared with calculations of chains of increasing length for the same Stokes shift ν [Fig. 3(c,d)], the latter after averaging over all the l_{gap}=0.9 nm gaps according to Eqn. (3). The calculated average SERS enhancement is equivalent to the total SERS signal measured

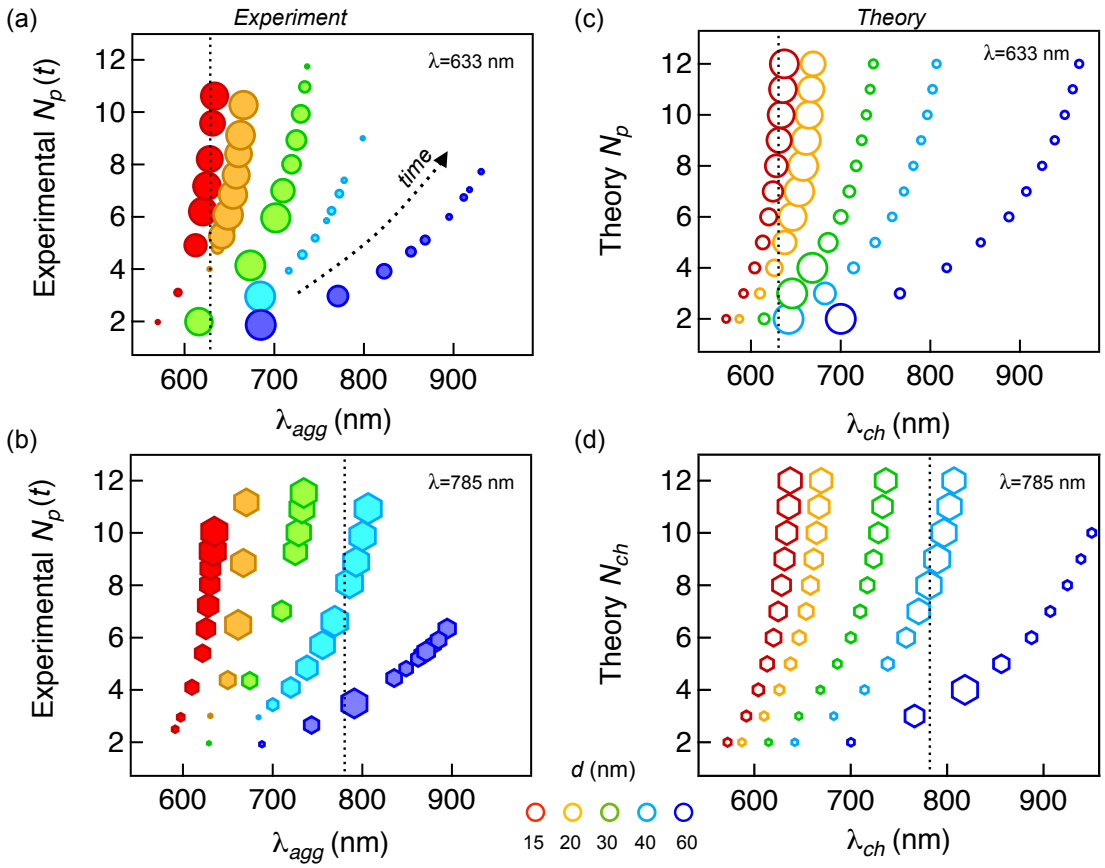

Figure 3: Theoretical and experimental dependence of the SERS signal on cluster size. (a,b) The measured SERS intensity for each nanoparticle size is plotted as the cluster grows against the extinction resonant wavelength λ_{agg} and against the corresponding effective length N_p for (a) λ=633 nm and (b) λ=785 nm. Each data set of a different color, corresponding to one particle size as given by the legend, is obtained for a Stokes shift of ν=826 cm^{-1}. The SERS signal is represented linearly by the area of the marker, where both the area of the smaller and larger symbols are identical for all data sets and independent of the absolute variation of the signal. The marker area and signal amplitude are thus not proportional, as the linear relationship involves an offset that depends on the particle diameter. (c,d) SERS intensity calculated from the nanochain as a function of length N_{ch} and resonant extinction wavelength λ_{ch} for (c) λ=633 nm and (d) λ=785 nm where both assume a Stokes shift of ν=826 cm^{-1} and we normalize in the same manner as in (a,b). The dash vertical lines mark the excitation wavelength λ. In all calculations, polarization of the incident field along the chain is assumed.

experimentally under the assumption that the number of contributing nano-gaps remains constant, which appears to be a valid approximation for our clusters.[52] The electric field is parallel to the chains in the calculations, to excite the longitudinal modes.

The results of this comparison are presented for λ=633 nm [Fig. 3(a,c)] and 785 nm [Fig. 3(b,d)], plotted for different nanoparticle diameters as a function of the resonant wavelength of the long wavelength peak of each aggregate (experiment: λ_{agg} or theory: λ_{ch}). Larger red-shifts correspond to growing structures, as can be seen in the vertical axis, which gives the length of the calculated chain (N_{ch}) or the effective length of the chains in the experimental aggregate (N_p). Here N_p, obtained from λ_{agg} as previously discussed, is useful when considering the measured signal in terms of the length of the constituent chains within the aggregates. The normalized integrated SERS intensity of each cluster is represented in Figure 3 by the area of the respective marker for both calculations and theory. The size of both the smallest and largest symbols is the same for all data sets, as we focus on the trends between these two limiting values, not on the magnitude of the change. Figures S2 and S3 in the supplementary information gives the SERS intensity normalized to the maximum for reference.

A very good qualitative agreement is found when comparing the evolution of the SERS enhancement with λ_{agg} from the experimental clusters and from the longitudinal modes of nanochains resonant at the same wavelength, i.e. we increase the length N_{ch} of the chain to equal the effective lengths N_p of long chains in the growing cluster. Notably, the measurements show a strong dependence of the optimal length on the diameter, which is nicely reflected by the calculations. Generally, the SERS enhancement is maximized when the detuning between the long wavelength plasmon and the illumination is small. This is shown in Figure 3 by the large values obtained for all d when the plasmon resonance is near the excitation wavelength (dashed line). To be more precise, the maximum can be found at slightly larger wavelengths than λ because of the Stokes shift and the need to optimize the

field enhancement at both input and output energy. The possibility to optimize SERS by minimizing the detuning with respect to the comparatively easy-to-track long wavelength extinction peak is of special interest for experiments.

According to the *ECM*, the optimization of the experimental signal for particular cluster sizes would then be explained by the presence of chains of effective length N_p that are resonant with the illumination wavelength.[53] The results are thus consistent with the *ECM*, which we initially developed to explain the far-field signal.[19] Nonetheless, to better assess the validity of the *ECM* to interpret Raman measurements it is convenient to look not only at the maximum enhancement, because although the SERS and the far-field can be essentially uncorrelated,[53] many models would predict a maximum SERS when illuminating near an extinction peak. Examining the decay of the Raman signal as the sizes deviate from the optimum, the agreement remains broadly satisfactory, supporting the *ECM* interpretation. We find particularly good qualitative agreement for the smaller nanoparticles (d=15 nm and 20 nm) of Figure 3 with λ=633 nm, and for sizes up to $d\approx$40 nm with λ=785 nm.

In contrast, for particle diameters where the illumination wavelength excites more efficiently the lowest energy mode of short chains, the calculations predict a sharper decay of the SERS enhancement as the length increases than that observed experimentally from growing clusters. We stress that Figure 3 shows how the signal from a given cluster varies between its maximum and minimum signal, not the absolute change. Notably, the change in the SERS from the experimental clusters in some cases can be much smaller than that calculated for the chains, for example seen with the largest particles (Supplementary Information, Fig. S3).

The *ECM* can also be used to qualitatively explain these disparities. Up to now, we have compared the experimental signal with the calculations from single chains. However, according to the *ECM*, it is generally necessary to consider longitudinal modes for both the chains of longer effective length and also dimers that appear at the periphery and remain

within the cluster throughout aggregation.[34] The nanocluster dimers can give a persistent and significant contribution to the SERS as the cluster grows, in strong contrast to the long-chain modes whose contribution varies depending on the extent of detuning. Chains shorter than N_p can also increase the background, while the SERS signal from single particle and transverse modes should be minimal.

Furthermore, when the resonance that exhibits weaker detuning with respect to the illumination is the long-chain mode, the optimization of SERS can be accounted for by only considering the behavior of a single chain. This would be the case for the smaller nanoparticles presented in Figure 3(a,b), particularly for λ=785 nm. In general however, one must consider both the contribution of the long embedded chains (containing N_p particles) *and* of the dimers and other shorter chains. Under resonant illumination the latter may contribute significantly, and even principally, to the overall SERS. This may be expected in particular when the incident wavelength strongly excites the dimer or a short chain resonance but not the long chain mode, as for $d \geq 30$ nm under λ=633 nm, where the dimer optimizes the SERS enhancement. In this case, the contribution from peripheral dimers to the experimental signal would lead to a relatively slow decay of the signal as the cluster grows, in comparison with the faster decay for the calculations of the growing chains. Using the *ECM*, we have thus been able to interpret the measured signal as coming from the different structural chains within the cluster.

Optimizing SERS when Λ=0: A simple model

In Figure 3 the Raman excitation wavelength was kept constant and the optimization of SERS was achieved for sizes of the aggregate that support the long wavelength resonance near this illumination frequency. An alternative scheme, and one which enables a larger SERS enhancement, is to change the Raman excitation wavelength as the structure grows so

that it always corresponds to the plasmon resonance (Λ=0). We consider now calculations of straight chains to better understand the SERS enhancement under these conditions. We model the chains with the experimental inter-particle gap of 0.9 nm and for simplicity assume a Raman shift of ν=0 cm^{-1}.

The SERS intensity calculated as a function of chain length and diameter for perfect Raman tuning (Λ=0) is presented in Figure 4(a). The Raman excitation wavelength given in Figure 4(a) corresponds to the wavelength of largest SERS, i.e. in this section the detuning is defined as the difference between the illumination wavelength and the wavelength for maximum SERS enhancement, corresponding to the longest wavelength mode. Previously, small detuning could be somewhat favourable for SERS enhancement (particularly for large ν) because Λ was defined with respect to the more easily measured extinction peak.

An essential result of Figure 4(a) is that for a given particle diameter the longest chain length is not necessarily optimal, as might have been expected.[54] For the smaller nanoparticles considered (d=10 nm-30 nm) which scatter weakly, indeed longer chains result in a stronger enhancement. Surprisingly however, for sufficiently large diameter particles ($d\geq$30 nm) long chains can be detrimental for yielding the largest SERS enhancement. For example, it is shown that for AuNPs with d=60 nm, the optimal chain length is the dimer, with the SERS intensity significantly reduced when adding additional nanoparticles to the chain.

A first possibility to explain the existence of an optimal length is to consider nanochains as one-dimensional Fabry-Pérot-like resonators.[54] Similar Fabry-Pérot cavity models have also been used for related plasmonic structures.[55–58] In this formalism, reflections at the chain end result in a plasmon oscillation comprising the entire chain. A maximum in the field enhancement thus occurs when, after one complete oscillation, the chain length is such as to allow the accumulated round-trip phase to be an integer multiple of 2π. For these resonances to be important, the accumulated absorption and scattering losses should be sufficiently low.

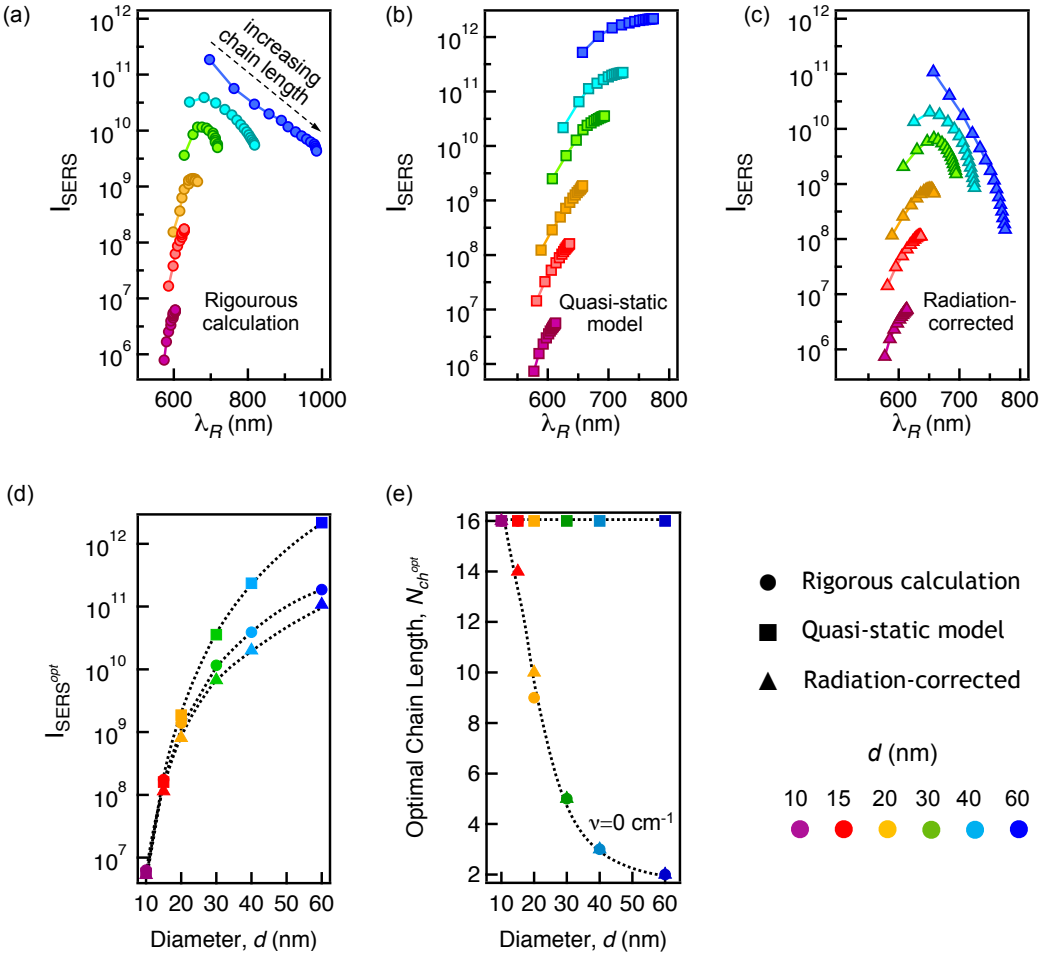

Figure 4: SERS intensity calculated for perfect tuning between the Raman excitation and the long wavelength nanochain mode for N_{ch}=2-16 with diameter d=10 nm-60 nm, calculated with (a) rigorous simulation, and using the model discussed in the text (b) before ('quasi-static') and (c) after ('radiation-corrected') radiative loss-correction. A scaling of f=0.1 is used in (b) and (c). We consider excitation at the wavelength that maximizes the SERS signal (zero detuning) for each chain length and no Stokes shift ν=0 cm^{-1} for (a) the full and (b-c) the quasi-static calculations without radiative correction. The results are expressed as a function of this excitation wavelength (notice the different wavelength range used) and, for each d, longer wavelengths correspond to larger chains. Panels (d) and (e) summarize the optimal chain length and SERS enhancement derived using the three approaches. (d) Chain lengths at which the enhancement is optimal and (e) corresponding maximum SERS enhancement for non-detuned excitation for various d. In all calculations, polarization along the chain axis is assumed.

We believe, however, that for the gold chains discussed here, these Fabry-Pérot-like resonator modes are strongly damped due to losses and cannot explain the results in Figure 4.

We describe in the following an alternative 'radiation-corrected' model in terms of a simple radiative (scattering) correction to the field enhancement of the chain. These radiation losses would reduce the signal for long chains of large particles[23,54] leading to the diminishing behavior observed in Figure 4(a). Before considering the full chain in this model, we initially introduce the simple case of a single sphere.[59–61] In the quasi-static approximation ($\lambda \gg d$) the enhanced field, $\left|E^{QS}\right|$, evaluated in this example at the point of largest enhancement, is given by

$$\left|\frac{E^{QS}}{E_0}\right| = \left|\frac{3\,\epsilon_{Au}}{\epsilon_{Au} + 2\epsilon_{wat}}\right| \tag{4}$$

where ϵ_{wat}=1.77 and ϵ_{Au} are the dielectric permittivity of the surrounding water and gold respectively, and $\left|E^{QS}\right|$ is normalized to the incident exciting field amplitude $\mid E_0 \mid$. The quasi-static dipole polarizability of the nanoparticle, α^{QS}, is given by:

$$\alpha^{QS} = \frac{\pi d^3}{2}\left(\frac{\epsilon_{Au} - \epsilon_{wat}}{\epsilon_{Au} + 2\epsilon_{wat}}\right) \tag{5}$$

These quasi-static expressions do not include the effect of scattering losses. To account for these losses we introduce a simple and often used radiative correction:[61,62]

$$\left|\frac{E^{RC}}{E_0}\right| = \frac{\left|E^{QS}\right|}{|E_0|\left|1 - i\frac{k^3}{6\pi}\alpha^{QS}\right|} \tag{6}$$

where k=$2\pi\sqrt{\epsilon_{wat}}/\lambda$ is the wavevector of the radiation in water. Alternative approaches to introduce scattering losses for the chain chain model have also been proposed.[63,64]

For the nanochains, incorporating an accurate radiative correction would require a careful treatment.[65] Instead, we follow here a first order approximation using the same radiative

correction [Eqn. (6)] as for the single sphere. The intention of this approach is to reproduce the main trends as the length of the chains and the size of the spheres are increased, without attempting exact quantitative agreement.

As a first step, we scale down all dimensions of the chain by a scale factor f=0.1 to largely suppress radiative losses. The parameter f should be sufficiently small for the scaled-down chains to be approximately in the quasi-static regime. To relate the resulting *scaled-down* quasi-static polarizability (α_{sd}^{QS}) to the quasi-static polarizability (α^{QS}) of the chain being analysed, we use the expression for dipolar modes in single particles:

$$\alpha_{sd}^{QS} = f^3 \alpha^{QS} \tag{7}$$

Further, using as a reference the behavior of simple systems, we consider the quasi-static fields to be size independent, such that before including retardation the enhancement of the scaled down (E_{sd}^{QS}) and normal sized (E^{QS}) chains are identical:

$$\left| \frac{E_{sd}^{QS}}{E^0} \right| = \left| \frac{E^{QS}}{E^0} \right| \tag{8}$$

Both α_{sd}^{QS} and E_{sd}^{QS} are obtained from full-electromagnetic BEM simulations of the scaled-down system. In particular, the scaled dipole polarizability α_{sd}^{QS} may be approximated from calculation of the extinction σ_{ext} and scattering σ_{sca} cross-section:[60]

$$Im(\alpha_{sd}^{QS}) = \frac{\sigma_{ext}}{k} \tag{9}$$

and

$$\left| \alpha_{sd}^{QS} \right| = \frac{\sqrt{6\pi\sigma_{sca}}}{k^2} \tag{10}$$

In which $Im()$ denotes the imaginary part. A subtlety in Eqn. (9) is that σ_{ext} is included

instead of the often used absorption cross section σ_{abs} because the scaled-down simulations do not completely suppress scattering.[66] In our case, this change modifies the results only negligibly. From α_{sd}^{QS} and E_{sd}^{QS}, the field enhancement before (E^{QS}=E_{sd}^{QS}) and after radiative correction (E^{RC}) is obtained using Eqns. (6-8). From E^{QS} and E^{RC}, it is then straightforward to get the corresponding Raman enhancement using Eqn. (3). We refer to the two sets of results as the 'quasi-static' and 'radiation-corrected' signal, respectively.

We present the resulting quasi-static [Figure 4(b)] and radiation-corrected [Figure 4(c)] SERS intensity for nanochains of various lengths and particle sizes, evaluated at the wavelength indicated by the horizontal axis. This wavelength corresponds in both cases to the quasi-static SERS peak, to avoid unphysical distortions of the spectra that can be introduced by our simplified radiative correction. The evolution of the resulting SERS enhancement can then be compared with the rigorous results by numerical simulation shown in Figure 4(a) at their corresponding resonant wavelength.

Firstly we note that for sufficiently large particles there is a clear deviation between the wavelength λ that optimizes SERS found from rigorous calculation [Figure 4(a)] and from the quasi-static results [used for both Figure 4(b) and Figure 4(c)]. We attribute these differences to the contribution to the interaction from higher order modes. These modes can play a role in the full simulations of the larger particles, but are expected to become much weaker in the scaled down system and thus in our quasi-static results. Neglecting this contribution to the interaction would explain the shorter resonant wavelengths. Here, however, we are interested in the qualitative evolution of SERS with N_{ch}, which, as Figure 4(b,c) shows can be well reproduced with the approximate expressions used.

Most notably, the evolution of the maximum SERS intensities with particle size and chain length shows very similar trends for our simple radiation-corrected model as for the rigorous calculation. In particular, both predict that similar chain lengths maximize SERS, with a

smaller number of particles being favorable as the diameter increases, from large chains of d=10 nm-20 nm to dimers of d=60 nm. This behavior is very different from the quasi-static result without radiative correction, which exhibits larger Raman signal for larger chains for all cases considered [see Fig. 4(b)]. Further, our simple model not only captures the optimal length, but it also gives a reasonable prediction of the absolute Raman signal for all lengths and diameters of the nanoparticles.

The discussed behavior is summarized in Fig. 4(d-e). Figure 4(d) shows the optimal length and Fig. 4(e) the corresponding SERS enhancement for this length at the optimal wavelength. The rigorous and the radiation-corrected calculations, which incorporate the effect of the scattering losses in different manners, give qualitatively and quantitatively similar trends, with an optimal length that decreases as the diameter of the constituent particles increases, the dimer being optimal for d=60 nm. In contrast, the quasi-static calculations finds the strongest signal for the largest number of particles N_{ch}=16. Further, the radiation-correction significantly reduce the total enhancement for the larger spheres, and so it emerges as an essential feature in modeling the nanochain SERS.

These findings support the dominant role of radiative losses in explaining the diameter-dependent optimal chain length for maximal Raman enhancement. The correction is negligible for small particles, where absorption strongly dominates over scattering, but becomes very substantial as the diameter of the spheres grow and the chain lengthens. An exact treatment may also be needed to consider the frequency-dependance of the dielectric function.[67] The radiative correction is expected to have a similar effect in the optimization of SERS for the more complicated experimental clusters,[68] especially taking into account the description of the aggregates in the embedded chain model as an ensemble of chains. However for such many-chain clusters, additional effects such as super-radiance from closely situated chains scattering coherently may increase the radiative losses, requiring careful correction.[65]

Summary and Conclusion

In this work, we have considered the problem of optimizing SERS from AuNP chains and clusters with fixed sub-nm gaps using two different schemes. In the first scheme, that considers a fixed SERS illumination wavelength, by performing measurements in real-time during the aggregation of AuNP:CB[5] clusters, we correlate the SERS signal with the long-wavelength resonance from the extinction spectrum. Optimum SERS is found when the cluster is of a size that presents a long-wavelength resonance near the excitation wavelength, an intuitive result that nonetheless cannot always be assumed.[53] The ability to predict optimal conditions in a growing cluster by using only the experimental far-field spectra allows advantageous feedback in design and control for sensing. We have shown how one may interpret nanocluster SERS using a simple embedded chain model that recasts the clusters into an appropriate ensemble of linear non-interacting nanochains.

While our focus is on the longest chains in the nano clusters, it is also useful for a fuller account of SERS to consider the presence of dimer modes at the periphery of the cluster. A more complete description of the experimental branched clusters would consider the contribution of the off- as well as on-resonant embedded chains of many different lengths, as well as the interactions between them. Such a fuller more complete description may be particularly convenient, for example, for more dense clusters such as those obtained from 'reaction-limited' regimes, that are not considered in this work.[33]

In a second approach, we find that when the Raman excitation wavelength can be freely tuned to a particular nanostructure, longer chains are still not necessarily optimal, and the optimal length varies sensitively as a function of nanoparticle size. We attribute these observations to radiative losses that become large for long chains and larger particles. To test this explanation, we developed a simple radiation-corrected model to estimate the effect that the radiation losses have on the Raman signal. We find a very good agreement in the

prediction of the optimal number of particles between the model and the exact calculations for all particle sizes considered. Similar considerations should apply to model the experimental nanocluster, although obtaining the necessary radiative corrections remains a difficult task.

Nonetheless, we believe the findings in this work should apply to many different branched clusters, independent of plasmonic material and nanoparticle size, at least for moderate size, well controlled gaps and little variability between the constituent particles. This work thus provides a key bridge between exact electrodynamic simulations and simple models which are based on experimental spectroscopy. Equally, optimization of the nanocluster near-field presented in this work can also form the basis for improved performance of the nanoclusters when used in applications such as plasmon-enhanced photochemistry and photocatalysis.[69−71]

Supporting Information

1. Protocols for AuNP-CB[5] aggregation
2. Extinction spectroscopy methodology and spectra, including mode decomposition and extraction
3. SERS spectra of AuNP:CB[5] solution and calculation of integrated SERS intensity
4. Comparison of the normalized integrated SERS signal with numerical calculations for a linear nanochain as a function of long wavelength resonance

Acknowledgement

This work was supported by EPSRC EP/F059396/1, EP/G060649/1 and EP/H007024/1 EU NanoSci-E+ CUBiHOLE grants, ERC LINASS, the ETORTEK 2014-2015 project COR-

ROPTO for the Department of Industry of the Basque Government, the project FIS2013-41184-P of the Spanish Ministry of Economy and Competitiveness MINECO, ETORTEK project nanoGUNE'14 from the Department of Industry of the Basque Government, the Fellows Gipuzkoa program of the Gipuzkoako Foru Aldundia (through the FEDER funding scheme of the European Union "Una manner de hater Europa") and the Physics Frontier Center at the Joint Quantum Institute, University of Maryland.

References

(1) Inoue, M.; Ohtaka, K. Surface Enhanced Raman Scattering by Metal Spheres. I. Cluster Effect. *J. Phys. Soc. Jpn* **1983**, *52*, 3853-3864.

(2) Blatchford, C. G.; Campbell, J. R.; Creighton, J. A. Plasma resonance: Enhanced Raman Scattering by Absorbates on Gold Colloids: The Effects of Aggregation. *J. A. Surf. Sci.* **1982**, *120*, 435-455.

(3) Savage, K. J.; Hawkeye, M. M.; Esteban, R.; Borisov, A. G.; Aizpurua, J.; Baumberg, J. J. Surface Plasmon Polaritons and Quantum Conductance in Nano-Tip Systems. *Nature* **2012**, *491*, 574-577.

(4) Xu, H.; Aizpurua, J.; Kall, M.; Apell, P.; Käll, M. Electromagnetic Contributions to Single-Molecule Sensitivity in Surface-Enhanced Raman Scattering. *Phys. Rev. E* **2000**, *62*, 4318-4324.

(5) Moskovits, M. Surface-Enhanced Raman Spectroscopy: A Brief Retrospective. *J. Raman Spectrosc.* **2005**, *36*, 485-496.

(6) Otto, A.; Mrozek, I.; Grabhorn, H.; Akemann, W. Surface Enhanced Raman Scattering. *J. Phys. Condens. Matter* **1992**, *4*, 1143-1212.

(7) Rechberger, W.; Hohenau, A.; Leitner, A.; Krenn, J. R.; Aussenegg, F. R.; Lamprecht, B. Optical Properties of Two Interacting Gold Nanoparticles. *Opt. Commun.* **2003**, *220*, 137-141.

(8) Guerrini, L.; Graham, D. Molecularly-Mediated Assemblies of Plasmonic Nanoparticles for Surface-Enhanced Raman Spectroscopy Applications. *Chem. Soc. Rev.* **2012**, *41*, 7085-7107.

(9) Kneipp, J.; Kneipp, H.; Kneipp, K. SERS: A Single-Molecule and Nanoscale Tool for Bioanalytics. *Chem. Soc. Rev.* **2008**, *37*, 1052-1060.

(10) Abalde-Cela, S.; Aldeanueva-Potel, P.; Mateo-Mateo, C.; Rodríguez-Lorenzo, L.; Alvarez-Puebla, R. A.; Liz-Marzán, L. M. Surface-Enhanced Raman Scattering Biomedical Applications of Plasmonic Colloidal Particles. *J. R. Soc. Interface* **2010**, *7*, 435-450.

(11) Adato, R.; Altug, H. In-situ Ultra-Sensitive Infrared Absorption Spectroscopy of Biomolecule Interactions in Real Time with Plasmonic Nanoantennas. *Nat. Commun.* **2013**, *4*, 1-10.

(12) Nie, S. Probing Single Molecules and Single Nanoparticles by Surface-Enhanced Raman Scattering. *Science* **1997**, *275*, 1102-1106.

(13) Kneipp, K.; Wang, Y.; Kneipp, H.; Perelman, L. T.; Itzkan, I.; Dasari, R. R.; Feld, M. S. Single Molecule Detection Using Surface-Enhanced Raman Scattering (SERS). *Phys.*

Rev. Lett **1997**, *78*, 1667-1670.

(14) Xu, H.; Bjerneld, E. J. Spectroscopy of Single Hemoglobin Molecules by Surface Enhanced Raman Scattering. *Phys. Rev. Lett.* **1999**, *83*, 4357-4360.

(15) Haran, G. Single-Molecule Raman Spectroscopy: A Probe of Surface Dynamics and Plasmonic Fields. *Acc. Chem. Res.* **2010**, *43*, 1135-1143.

(16) Le Ru, E. C.; Meyer, M.; Etchegoin, P. G. Proof of Single-Molecule Sensitivity in Surface Enhanced Raman Scattering (SERS) by Means of a Two-Analyte Technique. *J. Phys. Chem. B* **2006**, *110*, 1944-1948.

(17) Wei, H.; Xu, H. Hot Spots in Different Metal Nanostructures for Plasmon-Enhanced Raman Spectroscopy. *Nanoscale* **2013**, *5*, 10794-10805.

(18) van Schrojenstein Lantman, E. M.; Deckert-Gaudig, T.; Mank, A. J. G.; Deckert, V.; Weckhuysen, B. M. Catalytic Processes Monitored at the Nanoscale with Tip-Enhanced Raman Spectroscopy. *Nat. Nanotechnol.* **2012**, *7*, 583-586.

(19) Taylor, R. W.; Coulston, R. J.; Biedermann, F.; Mahajan, S.; Baumberg, J. J.; Scherman, O. A. In Situ SERS Monitoring of Photochemistry within a Nanojunction Reactor. *Nano Lett.* **2013**, *13*, 5985-5990.

(20) Kasera, S.; Biedermann, F.; Baumberg, J. J.; Scherman, O. A.; Mahajan, S. Quantitative SERS Using the Sequestration of Small Molecules Inside Precise Plasmonic Nanoconstructs. *Nano Lett.* **2012**, *12*, 5924-5928.

(21) Zhang, R.; Zhang, Y.; C., D. Z.; Jiang, S.; Zhang, C.; G., C. L.; Zhang, L.; Liao, Y.; Aizpurua, J.; Luo, Y.; Yang, J. L.; Hou, J. G. Chemical Mapping of a Single Molecule by Plasmon-Enhanced Raman scattering. *Nature* **2013**, *498*, 82-86.

(22) Bell, S. E. J.; McCourt, M. R. SERS Enhancement by Aggregated Au colloids: Effect of Particle Size. *Phys. Chem. Chem. Phys.* **2009**, *11*, 7455-7462.

(23) Fraire, J. C.; Pérez, L. A.; Coronado, E. A. Cluster Size Effects in the Surface-Enhanced Raman Scattering Response of Ag and Au Nanoparticle Aggregates: Experimental and Theoretical Insight. *J. Phys. Chem. C* **2013**, *117*, 23090-23107.

(24) Sztainbuch, I. W. The effects of Au Aggregate Morphology on Surface-Enhanced Raman Scattering Enhancement. *J. Chem. Phys.* **2006**, *125*, 124707-124712.

(25) Pustovit, V. N.; Shahbazyan, T. V. SERS from Molecules Adsorbed on Small Ag Nanoparticles: A Microscopic Model. *Chem. Phys. Lett.* **2006**, *420*, 469-473.

(26) Le Ru, E. C.; Etchegoin, P. G. Phenomenological Local Field Enhancement Factor Distributions Around Electromagnetic Hot Spots. *J. Chem. Phys.* **2009**, *130*, 181101.

(27) Banholzer, M. J.; Millstone, J. E.; Qin, L.; Mirkin, C. A. Rationally Designed Nanostructures for Surface-Enhanced Raman Spectroscopy. *Chem. Soc. Rev.* **2008**, *37*, 885-897.

(28) Esteban, R.; Taylor, R. W.; Baumberg, J. J.; Aizpurua, J. How Chain Plasmons Govern the Optical Response in Strongly Interacting Self-assembled Metallic Clusters of Nanoparticles. *Langmuir* **2012**, *28*, 8881-8890.

(29) Park, S. Y.; Lee, J.-S.; Georganopoulou, D.; Mirkin, C. A.; Schatz, G. C. Structures of DNA-Linked Nanoparticle Aggregates. *J. Phys. Chem. B* **2006**, *110*, 12673-12681.

(30) Girard, C.; Dujardin, E.; Li, M.; Mann, S. Theoretical Near-Field Optical Properties of Branched Plasmonic Nanoparticle Networks. *Phys. Rev. Lett.* **2006**, *97*, 100801.

(31) Sanchot, A.; Baffou, G.; Marty, R.; Arbouet, A.; Quidant, R.; Girard, C.; Dujardin, E. Plasmonic Nanoparticle Networks for Light and Heat Concentration. *ACS Nano* **2012**, *6*, 3434-3440.

(32) Tserkezis, C.; Taylor, R. W.; Beitner, J.; Esteban, R.; Baumberg, J. J.; Aizpurua, Optical Response of Metallic Nanoparticle Heteroaggregates with Subnanometric Gaps. *J. Part. Part. Syst. Charact.* **2014**, *31*, 152-160.

(33) Lin, M. Y.; Lindsay, H. M.; Weitz, D. A.; Ball, R. C.; Klein, R.; Meakin, P. Universal Reaction-limited Colloid Aggregation. *Phys. Rev. A* **1990**, *41*, 2005-2020.

(34) Taylor, R. W.; Lee, T.-C.; Scherman, O. A.; Esteban, R.; Aizpurua, J.; Huang, F. M.; Baumberg, J. J.; Mahajan, S. Precise Subnanometer Plasmonic Junctions for SERS Within Gold Nanoparticle Assemblies Using Cucurbit[n]uril "Glue". *ACS Nano* **2011**, *5*, 3878-87.

(35) Tao, C.-A.; An, Q.; Zhu, W.; Yang, H.; Li, W.; Lin, C.; Xu, D.; Li, G. Cucurbit[n]urils As A SERS Hot-Spot Nanocontainer Through Bridging Gold Nanoparticles. *Chem. Commun.* **2011**, *47*, 9867-9869.

(36) Lee, T.-C.; Scherman, O. A. Formation of Dynamic Aggregates in Water by Cucur-

bit[5]uril Capped with Gold Nanoparticles. *Chem. Commun.* **2010**, *46*, 2438-2440.

(37) Masson, E.; Ling, X.; Joseph, R.; Kyeremeh-Mensah, L.; Lu, X. Cucurbituril Chemistry: A Tale of Supramolecular Success. *RSC Adv.* **2012**, *2*, 1213-1247.

(38) Das, D.; Scherman, O. A. Cucurbituril: At the Interface of Small Molecule Host-Guest Chemistry and Dynamic Aggregates. *Isr. J. Chem.* **2011**, *51*, 537-550.

(39) Lin, M. Y.; Lindsay, H. M.; Weitz, D. A.; Ball, R. C.; Klein, R.; Meakin, P. Universality in Colloid Aggregation. *Nature* **1989**, *339*, 360-362.

(40) Lin, M. Y.; Lindsay, H. M.; Weitz, D. A.; Klein, R.; Ball, R. C.; Meakin, P. Universal Reaction-Limited Colloid Aggregation. *J. Phys. Condens. Matter* **1990**, *2*, 3093-3113.

(41) García de Abajo, F.; Howie, A. Retarded Field Calculation of Electron Energy Loss in Inhomogeneous Dielectrics. *Phys. Rev. B* **2002**, *65*, 115418.

(42) García de Abajo, F. J.; Aizpurua, Numerical Simulation of Electron Energy Loss Near Inhomogenous Dielectrics. *J. Phys. Rev. B* **1997**, *56*, 15873.

(43) Harris, N.; Arnold, M. D.; Blaber, M. G.; Ford, M. J. Plasmonic Resonances of Closely Coupled Gold Nanosphere Chains. *J. Phys. Chem. C* **2009**, *113*, 2784-2791.

(44) Citrin, D. S. Coherent Excitation Transport in Metal-Nanoparticle Chains. *Nano Lett.* **2004**, *4*, 1561-1565.

(45) Okamoto, H.; Imura, K. Visualization of Localized Intense Optical Fields in Single

Gold-Nanoparticle Assemblies and Ultrasensitive Raman Active Sites. *J. Phys. Chem. Lett.* **2013**, *4*, 2230-2241.

(46) Zuloaga, J.; Nordlander, P. On The Energy Shift Between Near-field and Far-field Peak Intensities in Localized Plasmon Systems. *Nano Lett.* **2011**, *11*, 1280-1283.

(47) Alonso-González, P.; Albella, P.; Neubrech, F.; Huck, C.; Chen, J.; Golmar, F.; Casanova, F.; Hueso, L. E.; Pucci, A.; Aizpurua, J.; Hillenbrand, R. Experimental Verification of the Spectral Shift Between Near- and Far-Field Peak Intensities of Plasmonic Infrared Nanoantennas. *Phys. Rev. Lett.* **2013**, *110*, 203902.

(48) Chen, J.; Albella, P.; Pirzadeh, Z.; Alonso-González, P.; Huth, F.; Bonetti, S.; Bonanni, V.; Akerman, J.; Nogués, J.; Vavassori, P.; Dmitriev, A.; Aizpurua, J.; Hillenbrand, R. Plasmonic Nickel Nanoantennas. *Small* **2011**, *7*, 2341-2347.

(49) Le Ru, E. C.; Blackie, E.; Meyer, M.; Etchegoin, P. G. Surface Enhanced Raman Scattering Enhancement Factors: A Comprehensive Study. *J. Phys. Chem. C* **2007**, *111*, 13794-13803.

(50) Le Ru, E. C.; Etchegoin, P. G. Annu. Single-Molecule Surface-Enhanced Raman Spectroscopy. *Rev. Phys. Chem.* **2012**, *63*, 65-87.

(51) Mahajan, S.; Cole, R. M.; Speed, J. D.; Pelfrey, S. H.; Russell, A. E.; Bartlett, P. N.; Barnett, S. M.; Baumberg, J. J. Raman and SERS Spectroscopy of Cucurbit[n]urils. *J. Phys. Chem. C* **2010**, *114*, 7242-7250.

(52) Taylor, R. W.; Esteban, R.; Mahajan, S.; Coulston, R.; Scherman, O. A.; Aizpurua, J.;

Baumberg, J. J. Simple Composite Dipole Model for the Optical Modes of Strongly-Coupled Plasmonic Nanoparticle Aggregates. *J. Phys. Chem. C* **2012**, *116*, 25044-25051.

(53) Kleinman, S. L.; Sharma, B.; Blaber, M. G.; Henry, A.-I.; Valley, N.; Gri, R.; Natan, M. J.; Schatz, G. C.; Van Duyne, R. P. Structure Enhancement Factor Relationships in Single Gold Nanoantennas by Surface-Enhanced Raman Excitation Spectroscopy. *J. Am. Chem. Soc.* **2013**, *135*, 301-308.

(54) Wang, Z. B.; Luk'yanchuk, B. S.; Guo, W.; Edwardson, S. P.; Whitehead, D. J.; Li, L.; Liu, Z.; Watkins, K. G. The Influences of Particle Number on Hot Spots in Strongly Coupled Metal Nanoparticles Chain. *J. Chem. Phys.* **2008**, *128*, 094705.

(55) Novotny, L.; Hecht, B. *Principles of Nano-Optics*; Cambridge University Press: Cambridge, U.K., 2006.

(56) Bozhevolnyi, S. I.; Sondergaard, T. General Properties of Slow-Plasmon Resonant Nanostructures: Nano-Antennas and Resonators. *Opt. Express* **2007**, *15*, 10869-10877.

(57) Sondergaard, T.; Beermann, J.; Boltasseva, A.; Bozhevolnyi, S. Slow-Plasmon Resonant-Nanostrip Antennas: Analysis and Demonstration. *Phys. Rev. B* **2008**, *77*, 115420.

(58) Bryant, G. W.; García de Abajo, F. J.; Aizpurua, J. Mapping the Plasmon Resonances of Metallic Nanoantennas. *Nano Lett.* **2008**, *8*, 631-636.

(59) Sarid, D.; Challener, W. *Modern Introduction to Surface Plasmons*; Cambridge University Press: Cambridge, U.K., 2010.

(60) Bohren, C. F.; Huffman, D. R. *Absorption and Scattering of Light by Small Particles*; John Wiley & Sons, Inc: New York, NY, 1998.

(61) Carminati, R.; Greffet, J.-J.; Henkel, C.; Vigoureux, J. M. Radiative and Non-Radiative Decay of a Single Molecule Close to a Metallic Nanoparticle. *Opt. Commun.* **2006**, *261*, 368-375.

(62) Wokaun, A.; Gordon, J. P.; Liao, P. F. Radiation Damping in Surface-Enhanced Raman Scattering. *Phys. Rev. Lett.* **1982**, *48*, 957-960.

(63) Bergamini, L.; Corni, S. Benchmarking Common Approximations for Determining the Particle-Size Dependence of Adsorbate-Induced Localized Surface Plasmon Resonance Shifts. *J. Phys. Chem. C* **2013**, *117*, 14742-14750.

(64) Schebarchov, D.; Auguié, B.; Le Ru, E. C. Simple Accurate Approximations for the Optical Properties of Metallic Nanospheres and Nanoshells. *Phys. Chem. Chem. Phys.* **2013**, *15*, 4233-4242.

(65) Le Ru, E.; Somerville, W.; Auguié, B. Radiative Correction in Approximate Treatments of Electromagnetic Scattering by Point and Body Scatterers. *Phys. Rev. A* **2013**, *87*, 12504.

(66) van de Hulst, H. C. *Light Scattering by Small Particles*; Courier Corporation: New York, NY, 1957.

(67) Wang, F.; Shen, Y. R. General Properties of Local Plasmons in Metal Nanostructures. *Phys. Rev. Lett.* **2006**, *97*, 206806.

(68) Le, F.; Brandl, D. W.; Urzhumov, Y. A.; Wang, H.; Kundu, J.; Halas, N. J.; Aizpurua, J.; Nordlander, P. Metallic Nanoparticle Arrays: A Common Substrate for Both Surface-enhanced Raman Scattering and Surface-Enhanced Infrared Absorption. *ACS Nano* **2008**, *2*, 707-718.

(69) Lining, S.; Christopher, P.; Ingram, D. B. Plasmonic-Metal Nanostructures for Efficient Conversion of Solar to Chemical Energy. *Nat. Mater.* **2011**, *10*, 911-921.

(70) Zhou, N.; Lopez-Puente, V.; Wanq, Q.; Polavarapu, L.; Pastoriza-Santos, I.; Xu, Q.-H. Plasmon-enhanced Light Harvesting: Applications in Enhanced Photocatalysis, Photodynamic Therapy and Photovoltaics. *RSC Adv.* **2015**, *5*, 29076-29097.

(71) Ueno, K.; Misawa, H. Surface Plasmon-Enhanced Photochemical Reactions. *J. Photoch. Photobio. C* **2013**, *15*, 31-52.